Structures and phase transitions in polar smectic liquid crystals

P. V. Dolganov, V. M. Zhilin, and V. K. Dolganov
Institute of Solid State Physics, Russian Academy of Sciences, 142432 Moscow Region, Chernogolovka, Russia

E. I. Kats
Laue-Langevin Institute, F-38042, Grenoble, France
and L. D. Landau Institute for Theoretical Physics, RAS, Moscow, Russia

(Received 16 October 2002; published 29 April 2003)

A discrete phenomenological model of antiferroelectric liquid crystals is used to study the structures and phase transitions in bulk samples and thin films. An important ingredient of our investigations is minimization of the free energy with respect to the phase and modulus of the order parameter. A simple version of the free energy, which contains only the nearest-neighbor and the next-nearest-neighbor layer interactions gives a complete phase diagram with all the observed smectic-C* (SmC^*) variant phases. In thin free-standing films, surface ordering may lead to suppression of the bulk SmC^*_α helix and to formation of planar structures. Transitions between these structures are accompanied by the 90° reorientation of the polarization direction. We also discuss the influence of chirality on subphase structures.

DOI: 10.1103/PhysRevE.67.041716 PACS number(s): 61.30.−v, 64.70.Md

I. INTRODUCTION

In recent years one of the most extensively studied phases of liquid crystals, both for basic research and for applications, are chiral polar smectics. The combination of chirality and polarity in tilted smectic liquid crystals results in many interesting structures, where these effects interplay. After the discovery of antiferroelectric smectic-C* (SmC^*_A) phase, short-pitch incommensurate SmC^*_α and several other subphases [1,2], it has become evident that a variety of phases with polar layers possessing unusual interlayer structures and physical properties is realized in liquid crystals. Significant experimental and theoretical efforts have been directed to investigate these new polar liquid-crystalline materials. However, until recent time, structures of only two polar phases, namely, the ferroelectric SmC^* [3] and the antiferroelectric SmC^*_A were well understood and firmly identified. In these phases, the long molecular axes are tilted by a polar angle θ with respect to the layer normal **z**. Orientational ordering of molecules in the smectic layer can be described by a two-dimensional (2D) vector $\boldsymbol{\xi}$ that is the projection of the nematic director **n** onto the layer plane (Fig. 1). In the SmC^* phase, the azimuthal angle φ is practically the same in neighboring layers (synclinic structure). In the SmC^*_A phase the molecules in adjacent layers are tilted in nearly opposite directions (anticlinic structure). Difficulties in studying the interlayer structure of other phases by conventional x-ray methods were due to the insensitivity of the diffraction along the Q_z reciprocal space direction to the tilt plane orientation in smectic layers. The breakthrough was achieved in 1998 when Mach *et al.* [4] conducted measurements of resonant x-ray scattering using a specially synthesized compound, in which the tensorial structure factor depended on the molecular orientation with respect to the polarization of the x-ray beam. It was shown [4,5] that the SmC^*_α phase possesses an incommensurate short periodicity from about five to eight layers. According to ellipsometric and optical reflectivity data [6–8], the azimuthal orientation of molecules can be described by a short-pitch helix with the axis perpendicular to the smectic layers. SmC^*_{FI1} and SmC^*_{FI2} have correspondingly three-layer and four-layer structures.

Several models have been proposed for the structure of the subphases. In the first Ising-like model [2,9,10], the structure of subphases was characterized by either synclinic or anticlinic ordering of molecules in a unit cell. The assumption that φ is either 0 or π was based on the known structure of the SmC^* and SmC^*_A phases with nearly coplanar ordering in neighboring smectic layers. Frustrating inter-

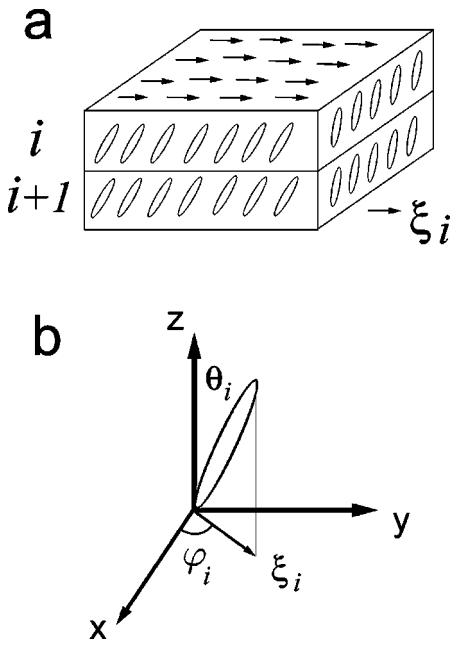

FIG. 1. Layer structure of a tilted smectic (a) and orientational ordering of molecules (b). θ_i and φ_i are the polar and azimuthal angles, the two-component vector $\boldsymbol{\xi}_i$ is the order parameter.

actions between layers which are assumed in this model may lead to different sequences of synclinic and anticlinic orientations in a unit cell. Inconsistence of these coplanar structures to experimental data lead to development of a so-called distorted Ising model [11] for subphase description.

The second model proposed by Pikin *et al.* [12–14] is based on the short-pitch mode approach. In this semiphenomenological model, the spatially inhomogeneous part of the free energy is taken as a series of harmonic functions corresponding to the short-pitch modes. The model gives a good description of the observed structures and their temperature sequence, but it cannot be easily adapted for the case of thin films.

The third proposed model for the subphases is based on the two-component order parameter $\boldsymbol{\xi}$, which is homogenous in the plane (XY) of each layer, and on antiferroelectric (A) interaction (I) between the next-nearest neighbor (NNN) layers (short names: ANNNIXY model or ''clock'' model) [15–19]. Antiferroelectric NNN interactions lead to frustrations and to formation of commensurate and short-pitch incommensurate structures that was confirmed by the x-ray and optical measurements [4–8].

However, up to now many general features of the subphase structures are not yet clear. For example, it was found that the pitch in the SmC_α^* phase could vary substantially even in similar compounds [20], have different temperature dependencies (increase or decrease with temperature) [4,20], and change continuously from the long pitch in the SmC^* to the short one in the SmC_α^* [21]. Recently, essential difference in the structure of the SmC_α^* phase in the bulk samples and in the thin films was reported [22–24]. Moreover, structures without the short-pitch helix were found in thin films. Transitions between these structures take place with a 90° change of the electric polarization direction [23,24]. The nature of modification of the SmC_α^* phase in thin films with respect to the bulk is not clear.

In this paper, the generalized ANNNIXY model was used to describe the possible phase diagrams, transitions, and different structures resulting from frustrations in bulk samples and thin films. The bulk phase sequences SmC^*(SmC_A^*)-SmC_α^*-SmA or SmC^*(SmC_A^*)-SmC_{FI1}^*-SmC_{FI2}^*-SmC_α^*-SmA observed in experiments can be obtained in the frame of this model by including into the free energy expansion the energetic barrier for azimuthal molecular reorientations.

In thin films surface ordering leads, as a rule, to suppression of the bulk SmC_α^* helix and to formation of sequence of planar structures. Such structures in thin films were observed experimentally [22–24]. Planar structures of two types were found in our calculations. The first one results from synclinic-anticlinic (for the low-temperature SmC^* phase) or anticlinic-synclinic (for the low-temperature SmC_A^* phase) reorientation in the center of the film, where the tilt angle is small. These transitions are also accompanied by the 90° reorientation of the polarization direction. Such transitions with the change of polarization directions (transverse to longitudinal and vice versa) were observed experimentally [23,24]. For some values of the interaction parameters, especially in thick films, the transitions between planar structures occur via twisted structures. The second type of transitions is induced by the surface and it takes place below the bulk SmC^*-SmC_α^* transition temperature. The reorientations occur between the second and the third layer from the surface. Because these reorientations hold near two surfaces, in thick films they do not result in the change of the polarization direction.

At the moment, very little is known rigorously about the subtle interplay between chirality and frustrations. It is usually assumed that molecular chirality that determines the sign of the helical structure in the SmC_α^* phase yields only a small contribution to the spacial helical modulation as the SmC^* (SmC_A^*) pitch is large. We show in this work that the presence of both chirality and frustrations may lead to interference between them, resulting in a substantial modification of the phases and in appearance of a SmC_α^*-like structure, which cannot appear in achiral systems.

The remainder of our paper is structured as follows. In Sec. II, we formulate the model and present the basic expressions necessary for our investigation. Besides in this section, we discuss some qualitative features of the structures, phase transitions between them, and physical meanings of parameters entering the model. Section III is devoted to the numerical study of the model. We present structures and phase diagrams in different ranges of the model parameters, sample thicknesses, and external conditions (for bulk samples in Sec. III A and for thin films in Sec. III B). In Sec. III C, we investigate the role of chirality, which in some cases can lead to strong effects even for a small magnitude of the chiral contribution. We end with some brief conclusions in Sec. IV.

II. THEORETICAL MODEL

In order for the later discussions to be made smoothly, we give here the qualitative description of our model. As we already mentioned in the preceding section, recent experiments resulted in the determination of the structures of polar liquid crystalline phases. Some of them can be theoretically described by continuous Landau-type models (see, e.g., Ref. [25], the monograph [26], and references herein). However, even for these phases the continuous Landau theory may not be applied to thin films composed of a small number of layers. To describe phase transitions and structures in polar smectic liquid crystals, we use the discrete phenomenological XY model with nearest-neighbor (NN) and next-nearest neighbor antiferroelectric interactions (ANNNIXY model) [15–19]. In this theory, smectic films are modeled as stacks of N layers with the two-component (i.e., 2D vector) order parameter $\boldsymbol{\xi}_i$, where i stands for the ith layer (Fig. 1). The free energy of an N-layer film can be written as an expansion over the structural ($\boldsymbol{\xi}$) and polar ($\mathbf{P}$) order parameters. Minimization of this energy with respect to the polarization $\mathbf{P}$ gives a relation between $\boldsymbol{\xi}$ and $\mathbf{P}$. So the final energy depends only on $\boldsymbol{\xi}$ with renormalized coefficients of the expansion.

The simplest base expansion of the free energy for coupled smectic layers with NN and NNN interactions [17–19] reads

$$F_0 = F_1 + F_2 + F_3, \tag{2.1}$$

where

$$F_1 = \sum_i \left[\frac{1}{2} a_0 \boldsymbol{\xi}_i^2 + \frac{1}{4} b_0 \boldsymbol{\xi}_i^4 + \frac{1}{8} a_2 \boldsymbol{\xi}_i \cdot \boldsymbol{\xi}_{i+2} \right], \tag{2.2}$$

$$F_2 = \frac{1}{2} a_1 \sum_i \boldsymbol{\xi}_i \cdot \boldsymbol{\xi}_{i+1}, \tag{2.3}$$

and

$$F_3 = b_1 \sum_i \boldsymbol{\xi}_i^2 (\boldsymbol{\xi}_{i-1} \cdot \boldsymbol{\xi}_i + \boldsymbol{\xi}_i \boldsymbol{\xi}_{i+1}). \tag{2.4}$$

In Eq. (2.2), $a_0 = \alpha(T - T^*)$ and b_0 are Landau coefficients describing the SmA to SmC transition in noninteracting layers. F_2 corresponds to the conventional gradient term $(d\boldsymbol{\xi}/dz)^2$ of the continuous Landau theory. In systems with planar tilted smectic phases $(d\boldsymbol{\xi}/dz)^2$ describes the fluctuations of the tilt θ. This contribution to the energy stabilizes the synclinic structures (SmC) for negative a_1 and anticlinic structures (SmC_A) for positive a_1. It is worth noting that in the systems under consideration with the vector order parameter this term is responsible not only for fluctuations of the modulus and of the phase of the order parameter but also for subphase formations. F_3 also describes the coupling between the neighboring layers. The last term in Eq. (2.2) may lead to frustrations of synclinic and anticlinic homogenous ordering in the system, since at $a_2 > 0$ it favors anticlinic orientation in next-nearest layers, which is incompatible with these homogenous structures. Due to these competing trends large a_2 results in the formation of compromise commensurate or incommensurate (SmC_α^*) structures releasing frustrations.

The physical meaning of different terms was discussed previously in the literature. F_2 is determined by a certain competition of conventional steric and van der Waals interactions that have different signs and favor synclinic and anticlinic ordering, respectively [27]. As was shown by Osipov and Fukuda [28], strong correlations between transverse molecular dipoles located in flexible chains can also be responsible for the anticlinic configuration. F_3 arises from the short-range dispersion and quadrupolar interactions. Likewise F_2, this term, depending on its sign, stabilizes synclinic (b_1 is negative) or anticlinic (b_1 is positive) ordering. The interaction $(\boldsymbol{\xi}_i \cdot \boldsymbol{\xi}_{i+2})$ coupling next-nearest layers may have different nature, in particular, it results from the large flexoelectric effect [27].

In our calculations, we also introduced some additional terms in the free energy expansion. It is known that taking into account the nearest-neighbor interaction only in a bilinear form, F_2, leads to formation of either SmC(SmC_A) phase at $|a_1/a_2| > 1$ or a short-pitch structure at $|a_1/a_2| < 1$ at all temperatures below the SmA [17–19]. The question thus arises whether a more reasonable model can be found that would predict the observed experimentally phase transition between SmC_α^* and SmC^*(SmC_A^*). To get this phase transition, one has to introduce a certain energetic barrier for azimuthal reorientations of molecules between synclinic and anticlinic structures. The simplest term providing such a barrier is

$$F_4 = a_3 \sum_i [\boldsymbol{\xi}_i \times \boldsymbol{\xi}_{i+1}]^2. \tag{2.5}$$

Due to the biquadratic interaction this term as well as F_3 is more essential at low temperatures, when the tilt angle is large.

The SmC_α^* phase is observed in compounds with chiral molecules. The chiral interaction is usually presented in the free energy by the so-called Lifshits term, which can be taken in the form

$$F_5 = f \sum_i [\boldsymbol{\xi}_i \times \boldsymbol{\xi}_{i+1}]_z. \tag{2.6}$$

In Secs. III A and III B, we present (unless the opposite is said) the results of our calculations without the chiral term and in Sect. III C, we investigate the effects induced by chirality. When the calculations are made without the chiral term, we shall use the notations without the star (e.g., SmC_α), and the star superscript denotes that the chiral term is introduced. When referring to experimentally observed phases, we shall use the traditional notations for chiral materials with the star.

It is established [29] that in some compounds the tilted smectic state can be very close to the Landau tricritical point, so for the correct description of the temperature dependence of the tilt order parameter θ, the sixth-order term in the free energy has to be taken into account

$$F_6 = c \sum_i \boldsymbol{\xi}_i^6, \tag{2.7}$$

where c (as well as α and b_0 above) should be positive. However, our numerical analysis (see the following section) shows that this term leads to some change of the temperature dependence of the order parameter, but does not alter qualitatively most of the results. Thus, in this work, unless otherwise stated, we present data obtained without the sixth-order term in the free energy.

In the films, there are two effects related to the existence of the surfaces. First effect is pure geometrical one. The surfaces break the translational and rotational invariance. Due to this fact the properties near the surface (and on the surface) should be different from the bulk properties. In our case, this geometrical factor is accounted automatically, via the missing part of NN and NNN interactions for the surface layers, and NNN interactions for the layers next to the surface. Besides certainly there are physical modifications of the system due to the existence of the boundaries. Surfaces can suppress the bulk ordering (this case is called the ordinary phase transition), surfaces can enhance the bulk ordering (it is called the extraordinary phase transition), or as a third possibility surfaces can experience their own intrinsic critical behavior (it is called the surface phase transition). There is also a special phase transition that is in some sense intermediate

between the ordinary and extraordinary phase transitions. To include the physical modification of the surfaces into our consideration, we took the first term of the free energy expansion F_1 for the surface layers in the form

$$\frac{1}{2}\alpha'(T-T_s)(\boldsymbol{\xi}_1^2+\boldsymbol{\xi}_N^2), \tag{2.8}$$

where T_s is the surface transition temperature in the film without interlayer interactions. The validity of such a modeling of the surface effects will be discussed in Sec. III B.

In Sec. III, we present the results of the numerical study of the model, namely, the equilibrium structures and phase diagrams in different ranges of the model parameters, sample thicknesses, and external conditions (for the bulk samples in Sec. III A and for the thin films in Sec. III B). In Sec. III C, we investigate the role of chirality, which can lead to noticeable effects even for a small magnitude of the chiral contribution into the free energy expansion.

Minimization of the free energy was performed by projected gradient quasi-Newton limited memory algorithm of bound-constrained optimization [30]. The developed numerical code allowed us to conduct calculations using simultaneously all listed terms in the free energy (2.1)–(2.8). However, analysis of the above model, as a rule, was performed using a limited number of terms in the free energy, to disentangle the influence of different terms on the possible equilibrium structures and phase transitions.

III. CALCULATIONS

A. The bulk phase diagrams

The short-pitch structure (SmC_α, SmC_α^*) appears in the case of frustrating interactions, i.e., at $a_2>0$, and only this case will be examined in our paper. In this section we study the influence of F_2, F_3, and F_4 terms and their combinations on the formation of the subphases and their structural properties. Here and below, we set b_0 equal to 1, thus employing the units with α measured in 1/K and keeping all the other coefficients dimensionless. The value of α was chosen, so that the order parameter modulus θ was 0.3–0.4 rad at $\Delta T = 10$ K below the phase transition from the bulk Sm*A* to the tilted phase (these magnitudes of θ are typical for Sm*C* liquid crystals).

It is worth mentioning that the full investigation of the phase diagrams even in the case of a limited number of interlayer interactions, requires considerable amounts of computational work. Frustrations can lead to formation of various nontrivial structures. It is one of the reasons why in spite of a number of publications a complete analysis of the roles of different terms in the free energy expansion is still not available. Moreover, most of the previous calculations were made, as a rule, under some simplifying assumptions (e.g., linear dependence of the order parameter phase φ on **z**, constancy of θ in different layers), which restricted the variety of possible equilibrium structures in the phase diagrams.

In the present work, the calculations of the structures and of the phase transitions were performed by means of minimization of F both over θ_i and φ_i in all layers of the film (i runs from 1 to N). To find the global minimum, minimization was repeated from 100 to 1000 times for random input trial structures. To determine the bulk phase diagrams, we take the film thicknesses up to 200 layers and the surface term (2.8) was taken the same as in the bulk (i.e., $\alpha' \equiv \alpha$, and $T_s \equiv T^*$). We believe that this approach enables us to catch all essential features of the bulk behavior. For $N > 25$, we did not find any essential variation of the parameters of all the resulting structures in the middle part of the film. Besides, we conducted a check of the structures and phase transition temperatures for the bulk sample: the minimum of the free energy for an infinite sample was found from a set of trial structures, obtained in the central part of the thick films. The accordance between the results obtained by these two methods was sufficiently good (e.g., the phase transition temperatures coincided with the accuracy better than 0.2 K). Formally, our procedure is not totally exhaustive with respect to all possible structures (e.g., there is no exact minimization algorithm for incommensurate structures). However, good agreement between the values of θ_i, φ_i, and the phase transition temperatures obtained by the both methods, enables us to assume that we did not lose any structure in our method of the calculations.

To confront our predictions with experimental observations, we always use temperature as one of the coordinates of the phase diagrams. This allows us to compare more easily the results obtained in our simulations with existing experimental data.

1. Phase diagram for the free energy $F=F_1+F_2+F_4$

The free energy in the form (2.2) upon decreasing temperature yields a phase transition from Sm*A* to a tilted structure, in which the rotation of $\boldsymbol{\xi}_i$ from layer to layer is determined by the frustration term $a_2\boldsymbol{\xi}_i\cdot\boldsymbol{\xi}_{i+2}$, i.e., anticlinic orientation of NNN layers. The rotation of the tilt plane between NN layers is not fixed by these terms. The interlayer interactions between NN layers (F_2) determine the angles between the tilt planes: for a large absolute value of a_1, namely, at $|a_1/a_2|>1$, the structure of the tilted phase is synclinic ($a_1<0$) or anticlinic ($a_1>0$). At $|a_1/a_2|<1$, the structure is formed with rotation of the tilt from layer to layer. It might seem that this phase resembles the short-pitch SmC_α^* phase, but independence of $\Delta\varphi=\varphi_{i+1}-\varphi_i$ on temperature [$\Delta\varphi=\arccos(-a_1/a_2)$] [19] and absence of the phase transition to the SmC(SmC_A) phase, disagrees with the experimental data. The phase sequence SmC-SmC_α-Sm*A* may be obtained upon introducing into the free energy the term F_4, which provides the energetic barrier between synclinic and anticlinic ordering.

Figure 2 shows a typical phase diagram in coordinates $T-T_0$ and a_1/a_2, where T_0 is the transition temperature from the Sm*A* to any tilted phase. The phase diagram was calculated for different values of the parameter a_1. The other parameters have been taken as $\alpha=0.01$ K^{-1}, $a_2=0.02$, $a_3=0.05$. In presence of the barrier F_4, the SmC(SmC_A) structure is formed both at $|a_1/a_2|>1$ and at $|a_1/a_2|<1$. In the SmC_α phase near the phase transition to the Sm*A* structure, the pitch is almost insensitive to F_4, i.e., the same as it

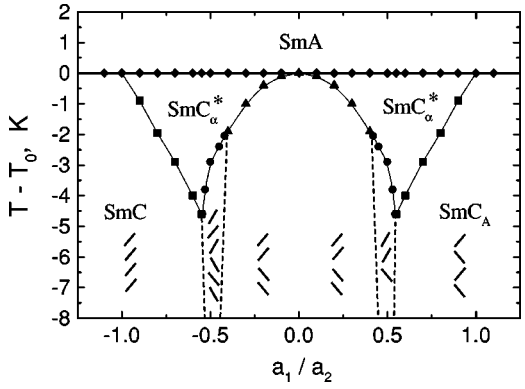

FIG. 2. Bulk phase diagram for the free energy in the form $F=F_1+F_2+F_4$. T_0 is the temperature of the transition from the Sm*A* to tilted phases. The set of model parameters is $\alpha=0.01\ \mathrm{K}^{-1}$, $a_2=0.02$, $a_3=0.05$. A schematic representation of the tilted structures appearing below the SmC_α phase is shown in the lower part of the figure.

would be without this term (as it should be because F_4 is the fourth-order term over the order parameter). As one can expect, when the interlayer interaction F_2 is decreased, the width of the SmC_α phase is increased and a four-layer structure is formed near $a_1/a_2=0$. However, the transition from Sm*C* to the four-layer structure occurs via an intermediate phase (Fig. 2). In the case of positive a_1 it is a three-layer structure, in the case of negative a_1 it is a six-layer one. All these four-, three-, and six-layer structures upon taking into consideration the chirality become nonplanar, and the four-layer and the three-layer structures can be considered as analogs of SmC^*_{FI2} and SmC^*_{FI1} phases. At an appropriate choice of the model parameters, we can obtain the same temperature sequences of the structures as those observed in experiments [see Sec. III B 2 and Fig. 4(b) with the schematic representation of the nonplanar structures]. The difference between the four-layer and the three-layer (or the six-layer) structures is not reduced to the pure quantitative fact that they have different periods. There is also a qualitative difference, manifesting itself in the fact that in the four-layer structure only the phase of the order parameter is varied, whereas in the three-layer and in the six-layer structure both the phase and the modulus of the order parameter are varied. The newly predicted six-layer structure has not been observed experimentally so far. Like in the three-layer structure, in the six-layer one, the order parameter modulus θ_i is varied in different layers. The tilt angle θ_i is larger in the layer that has the same ordering with respect to the both adjacent layers (two anticlinic for the three-layer, two synclinic for the six-layer cell). The both (three- and six-layer) structures are different from each other by the variation of the order parameter phase in the unit cell, however, if one takes into consideration only the order parameter modulus, the periodicity of the both structures is equal to three layers. This means that nonresonant x-ray diffraction sensitive to the difference in θ_i (and hence to the layer thickness $d_i=d_0\cos\theta_i$) is similar for the both structures.

Because many different models have been proposed, the ability to discriminate experimentally the actual molecular arrangements is critically important. One of the possibilities would be the observation of nonresonant x-ray scattering related to the layer thickness modulation. These satellite peaks should appear at the wave vectors $Q_z=Q_0(n\pm\frac{1}{3})$, where $Q_0=2\pi/\overline{d}$, $\overline{d}$ is the average layer thickness. The most intensive peaks in the six-layer structure are at $Q_z=2Q_0/3$ and $Q_z=4Q_0/3$, i.e., the same as in the three-layer structure [31]. Assuming a simple sinusoidal electron density modulation within each smectic layer, we can easily find the ratio (with respect to the main harmonic at $Q_0=2\pi/\overline{d}$) of Fourier harmonic amplitudes modula

$$\frac{A_{2/3}}{A_0}=\frac{36\sqrt{3}}{25\pi}\frac{\Delta d}{\overline{d}} \tag{3.1}$$

for $Q_z=2Q_0/3$ and

$$\frac{A_{4/3}}{A_0}=\frac{72\sqrt{3}}{49\pi}\frac{\Delta d}{\overline{d}} \tag{3.2}$$

for $Q_z=4Q_0/3$, where Δd is the difference in the layer thicknesses. Equations (3.1) and (3.2) were obtained by calculating electronic density Fourier harmonics in a linear over $\Delta d/\overline{d}$ approximation. We assume sinusoidal electronic density modulations for layers, and the layers differ in their thicknesses (the sequence is d, d, $d-\Delta d$, d, . . .). Peaks at $Q_z=Q_0(n\pm\frac{1}{6})$ related to the change of the order parameter phase could be observed only by means of resonant scattering.

Approaches to the theory of polar smectic phases similar to ours have been made by other authors, but some important differences from our work should be noted. The three-layer structures like we found above have been obtained previously in models, which included interactions between nearest neighboring (NN), next-nearest neighboring (NNN), and next-next-nearest neighboring (NNNN) layers [32,33]. We performed the minimization of the free energy over both the phase and the modulus of the order parameter. In this case, there is no need to invoke long-range interactions (namely, $\boldsymbol{\xi}_i\cdot\boldsymbol{\xi}_{i+3}$) to get the stable three-layer structure. In our model, it stems from only NN and NNN interactions. If one fixes the modulus of the order parameter in the smectic layers, three-layer structure would not appear in the model including only NN and NNN interactions. Thus, nonuniformity of θ_i in different layers is essential not only for the correct description of the structure, but also for the very existence of the three-layer phase itself. This variation of the order parameter modulus stems directly from the symmetry of the three-layer structure, i.e., it should be expected to appear at the correct minimization of the free energy.

One more specific feature of the presented phase diagrams is the structural difference of the SmC_α phase for positive and negative values of a_1. This possibility (i.e., existence of different types of SmC_α) was pointed in a recent publication [32]. In our case, at $a_1<0$ the pitch increases when the temperature decreases, therefore the SmC_α helix is unwound at the transition to the Sm*C* phase. At $a_1>0$ near the transition into the SmC_A phase, the local SmC_α structure resembles an

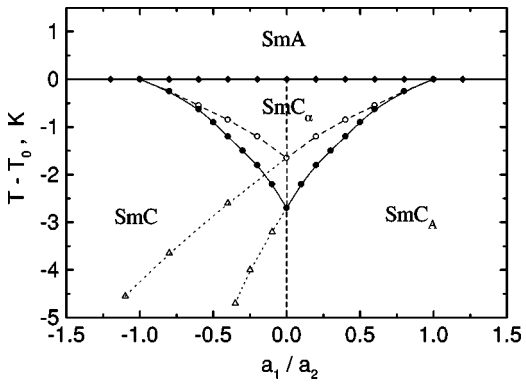

FIG. 3. Open circles represent the bulk phase diagram for the free energy in the form (2.1). T_0 is the temperature of the SmA-SmC_α or SmA-SmC(SmC_A) phase transitions. The model parameters are $\alpha=0.006\ \mathrm{K}^{-1}$, $a_2=0.005$, $|b_1|=0.07$. Closed circles represent the phase diagram with the sixth-order term F_6 (2.7). The model parameters are $\alpha=0.01\ \mathrm{K}^{-1}$, $a_2=0.02$, $|b_1|=0.1$, $c=0.5$. b_1 is positive in the right half of the diagram and negative in the left one. The triangles and the dashed lines represent the diagram for the low-temperature antiferroelectric phase with positive b_1 in the whole region of the phase diagram.

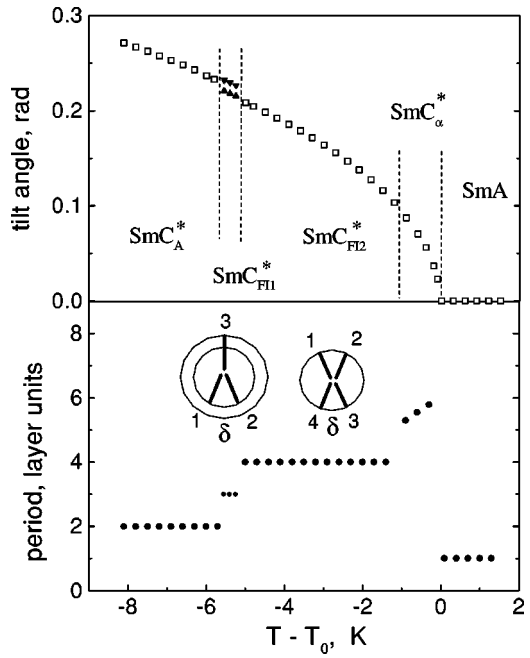

FIG. 4. The tilt angle (a) and cell period (b) versus temperature in SmC_A^*, SmC_{FI1}^*, SmC_{FI2}^*, SmC_α^* (incommensurate) phases. A schematic representation of the nonplanar three- and four-layer structures is shown in the upper part of (b). The distortion angle δ appears due to chirality. Up and down triangles in (a) correspond to layers denoted by 3 and 1 (2) in (b). The set of the model parameters is $\alpha=0.01\ \mathrm{K}^{-1}$, $a_1=-0.002$, $a_2=0.004$, $b_1=0.02$, $c=0.5$, $a_3=0.01$.

anticlinic one twisted in a long helix. The pitch of this helix (as well as for $a_1<0$) decreases with the temperature. However, this argumentation makes sense only for the case of quite long pitches. When the pitch decreases substantially, we cannot any longer describe the system in terms of anticlinic ordering of adjacent layers and of a pitch for the anticlinic pairs. It can be done in the SmC_A^* phase where the helix concerns the twist of anticlinic pairs, and for the SmC_A^* no disagreement exists as the pitch of the SmC_A^* helix is much larger than the layer spacing. At $a_1>0$ a continuous evolution of the helix in the whole temperature interval will be described if we follow the twist of the single layers. In this case, the SmC_α^* pitch in the low-temperature region only slightly exceeds the two layers distance and it increases with the temperature. Such temperature behavior of the SmC_α pitch at $a_1>0$ is opposite to the case with $a_1<0$. It is worth mentioning that for different compounds the both types of the behavior (decrease and increase of the pitch with the temperature) have been observed [4–8].

2. Phase diagram and structures for the free energy $F=F_0$, $F=F_0+F_6$, and $F=F_0+F_4+F_6$

An alternative scenario to obtain the SmA-SmC_α-SmC(SmC_A) phase sequence is related to the term F_3 in the free energy expansion. Figure 3 shows the phase diagram for the free energy F_0 (diamonds and open circles). Likewise in the previous case, the SmC_α phase appears at $|a_1/a_2|<1$. The sixth-order term ξ_i^6 in the free energy ($F=F_0+F_6$) somewhat modifies the temperature dependence of the SmC_α-SmC(SmC_A) phase transitions but does not qualitatively change the shape and topology of the phase diagram. Closed and open circles represent the phase diagram when both a_1 and b_1 change their signs at $a_1=0$. The triangles and the dashed lines show the SmC_A phase boundary when b_1 remains positive in the left part of the diagram. In this case, SmC_A phase exists below the dashed lines. The appearance of the structures depends on the ratio a_1/a_2. At a relatively large $|a_1/a_2|$, (in the case of a_1 negative, b_1 positive), besides the SmC_A, other commensurate structures exist. Even a richer phase diagram is obtained with the barrier term F_4. Figure 4 shows an example of the temperature dependence of the tilt angle and the cell parameter of the structures. Introduction of the Lifshits term results in the formation of nonplanar structures shown in the upper part of Fig. 4(b) (view along **z** axis). Optical data [6–8,34] indicate that the azimuthal orientation arrangement in the SmC_{FI1}^* phase presents a distorted clock structure and that the polar symmetry is quite large [34]. The angle δ is from about 30° to 57° [6–8,34]. The structures (Fig. 4) appear in the sequence observed in the classical antiferroelectric material MHPOBC in samples with high optical purity [33]. As we mentioned earlier, in the three-layer structure the tilt angle is not a constant in different layers [up and down triangles in Fig. 4(a)]. The tilt angle is larger in the layer with molecular orientations closer to anticlinic [orientation of the tilt plane denoted by 3 in Fig. 4(b)]. Dynamical light scattering measurements [34] show that the interlayer interaction coefficients in the free energy might be of comparable magnitude to intralayer coefficients. This important conclusion about the interlayer interaction confirms the validity of our calculations of the

SmC^*_{FI1} phase structure because the variation of θ_i in different layers is due to the interlayer interactions. The difference in the order parameter modulus θ_i in different layers is decreased when δ is increased and it gets down to zero at $\delta = 120°$ (the symmetric ''clock'' configuration). However, as it was experimentally established, the three-layer structure is not symmetric ($\delta \neq 120°$), and hence one should expect the difference of θ_i in the layers of the SmC^*_{FI1} phase.

Summarizing the results of the phase diagram calculations we can state that the main features of the SmC^*_α phase may be described using one of the terms of the fourth order (F_3 or F_4), but for full description of all smectic subphases other terms (F_3, F_4, and F_5) have to be regarded in the free energy expansion. In the phase diagrams, the stability lines are symmetric about $a_1/a_2=0$ but the structures of subphases may be different. However, even in this case a specific symmetry exists. Two structures appearing at the equal values of $|a_1/a_2|$ are similar in the following sense: if in the left part of Fig. 2 ($a_1<0$), we change the synclinic orientation in neighboring layers to anticlinic and vice versa, we will obtain the structure of the right part of the figure. For example, the six-layer structure (Fig. 2, left part) will become the three-layer structure.

B. The structures and transitions in thin films

As it was explained before, the physical modification of the surface layers with respect to the bulk ones was taken into consideration by the surface free energy (2.8). Different conditions on the surface may lead to increase [35,36] and to decrease [19,36] of the transition temperature from Sm*A* to the tilted phases with respect to the bulk sample. It is well established experimentally that the tilted structures in the films are observed at higher temperatures than in the bulk samples, both for synclinic and anticlinic ordering. It can be understood, since due to fairly large surface tension surface fluctuations of the order parameter are considerably hindered in the films and it increases the surface transition temperature T_s. In our calculations, we took T_s such that the temperature difference between the transitions Sm*A*-tilted phases in the two-layer films and in the bulk sample is equal to the experimentally observed value 30 K [35]. Our numerical results show that a variation of the parameter α' in some natural limits (within about 40%) induces some shift of the transition temperatures in the films but does not lead to a qualitative change of the equilibrium structures and of the sequence of the transitions. Due to this reason and for the sake of simplicity, the results presented in this section were obtained at the same value of α' as for the interior layers of the film.

Figure 5 shows the tilt angle profile θ in a six-layer film for a set of parameters corresponding to the phase diagram of Fig. 3 for $|a_1/a_2|=0.4$ (with the sixth-order term taken into account). The calculations were performed for the synclinic [$a_1/a_2=-0.4$, Fig. 5(a)] and anticlinic [$a_1/a_2=0.4$, Fig. 5(b)] low-temperature structures. Without the chiral term, these synclinic and anticlinic structures remain planar. Surface ordering results in a certain increase of the molecular tilt angle from the center of the film to the surface. At the temperatures slightly exceeding the bulk SmC(SmC_A)-SmC_α

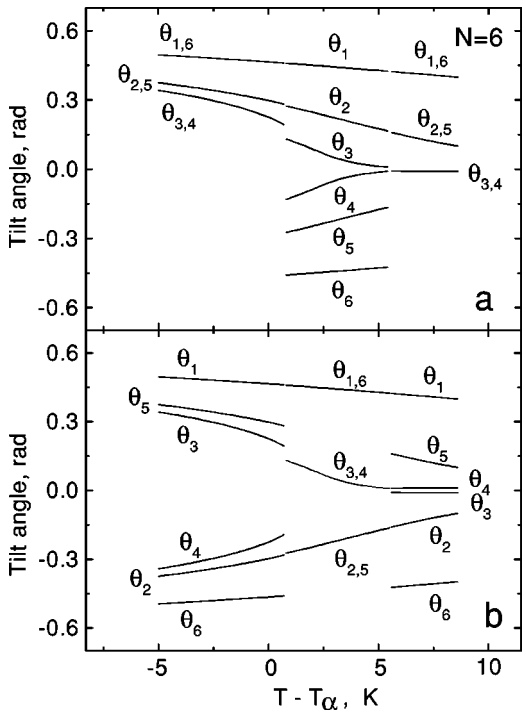

FIG. 5. Tilted planar structures in six-layer films for the case of low-temperature synclinic (a) and anticlinic (b) phases. The subscripts of θ_i denote the layer number within the film. These structures occur for the phase diagrams shown in Fig. 3. The data in the figure correspond to the case of the free energy with the sixth-order term and $|a_1/a_2|=0.4$. Transitions occur with the 90° change of the polarization direction.

transition temperature, reorientation of the tilt planes occurs in the film (Fig. 5). The relative direction of the molecular tilt in two central layers changes to the opposite: synclinic to anticlinic [Fig. 5(a)], anticlinic to synclinic [Fig. 5(b)]. However, the azimuthal interlayer ordering in the other parts of the films is not changed. In the case depicted in Fig. 5 the transition occurs in a stepwise manner, below and above the transition the structures are planar. The structures without the short-pitch helix were recently observed in compounds with the SmC^*_α phase [22–24]. In *N*-even films after the transition, θ in the central part of the film remains nonzero. In *N*-odd films (Fig. 6), $\theta=0$ in the central layer. If we include also the chiral Lifshits energy, it will lead to a small nonzero tilt in the central layer. However, even in the case of zero tilt, the orientations of the upper and lower halves of the film are correlated due to the NNN interactions: the anticlinic orientation of next-nearest neighbors is obtained both for the case of the low-temperature synclinic and anticlinic structures (Fig. 6).

Figure 7 shows the transition temperatures for different film thicknesses. The transitions from SmC or SmC_A occur when θ in the center of the film is sufficiently small, i.e., when NNN frustrating interactions become comparable to NN interactions. This phenomenon increases the phase transition temperatures upon decreasing the film thickness.

At further temperature increase a second phase transition occurs (Fig. 5). This transition temperature also increases as

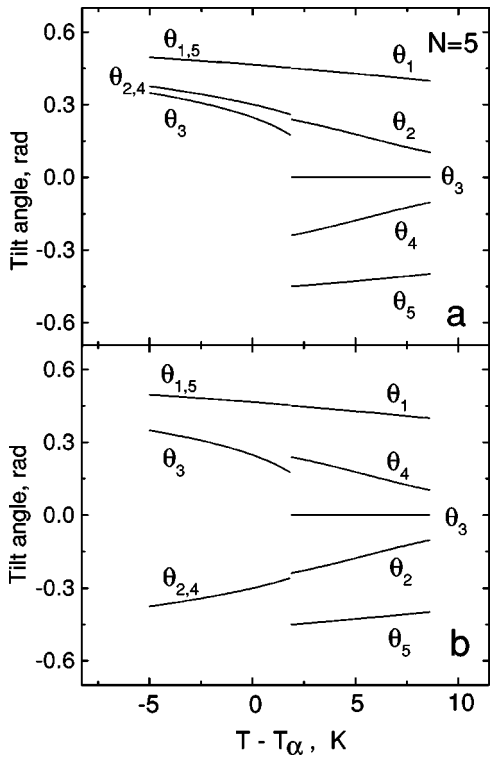

FIG. 6. Tilted planar structures in five-layer films for the case of low-temperature synclinic (a) and anticlinic (b) phases. The subscripts of θ_i denote the layer number in the film. These structures occur for the phase diagrams shown in Fig. 3. The data in the figure correspond to the case of the free energy with the sixth-order term and $|a_1/a_2|=0.4$. Transitions occur with the 90° change of the polarization direction.

the film thickness decreases (for the five-layer film the second transition takes place outside the temperature scale of Fig. 6). Likewise for the first transition, the corresponding structure remains planar. Thus, the bulk SmC_α phase is replaced in thin films by the series of transitions between a

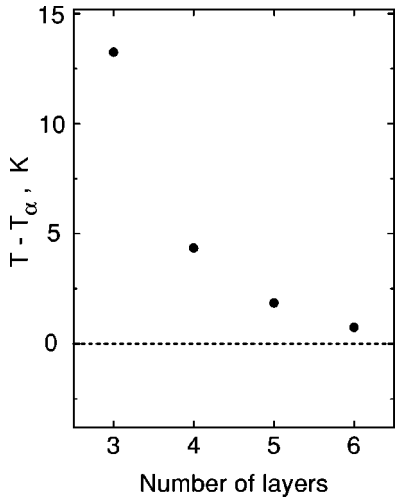

FIG. 7. Temperatures of the transition from the low-temperature ferroelectric or antiferroelectric state for different film thickness. The set of parameters is as in Figs. 3, 5, and 6.

number of planar structures. Such kind of the behavior (as well as even-odd alternations) was experimentally observed in the films of different thicknesses [23,24]. At the transitions, the symmetry of the film with respect to its center changes: antisymmetric-symmetric-antisymmetric for the low temperature synclinic state [Fig. 5(a)], symmetric-antisymmetric-symmetric for the low-temperature anticlinic state [Fig. 5(b)]. For the polar structures, such variations of the symmetry should lead to 90° change in the direction of the net polarization in the films irrespective, to a nature of polarization emerging in the films. The polarization direction is governed by the film symmetry: in the symmetric structures **P** is parallel to the molecular tilt plane, in the antisymmetric structures it is perpendicular to the molecular tilt plane.

Some comments concerning the polarization seem in order here. Let us consider first the simplest case when the low-temperature structure is synclinic [Figs. 5(a) and 6(a)]. In such a state in polar structures the polarization is perpendicular to the molecular tilt plane (transverse polarization $\mathbf{P}_\perp$ of the ferroelectric smectic). After the first transition the polarization becomes longitudinal $\mathbf{P}_\parallel$ (parallel to the molecular tilt plane). The next transition is again to the state with the transverse polarization. Longitudinal polarization emerges from the interlayer polarization parallel to the molecular tilt plane [28,37] and from the surface polarization. In the structure appearing after the first transition [Figs. 5(a) and 6(a)] in the upper and the lower halves of the film, the transverse polarizations point in the opposite directions, i.e., compensate each other. On the contrary, the directions of the longitudinal polarization in the upper and the lower parts of the film are the same, thus net $\mathbf{P}_\parallel \neq 0$. Analogous consideration is also appropriate for all other structures.

More tricky is the situation for the sequence of states emerging from the anticlinic structure [Figs. 5(b) and 6(b)]. Even in the antiferroelectric state the film symmetries are different [38,39]: symmetrical structures in *N*-even films and antisymmetrical ones in *N*-odd films. The symmetry analysis of the anticlinic structures given in the papers by Link *et al.* is conformed with the experiments performed by the same group [38,39]. Our calculations for *N*-even films give the following sequence of the structures [Fig. 5(b)]: symmetric (longitudinal polarization)-antisymmetric (transverse polarization)-symmetric (longitudinal polarization). In the *N*-odd films the symmetry of the structures is the opposite, and, consequently, the polarization direction is rotated by 90°. Such a sequence of the polarization directions at the transitions in the *N*-odd and *N*-even films was really observed in the films of the antiferroelectric liquid crystal with the SmC^*_α phase in the bulk sample [23,24].

We found the reorientation in the center of thin films in a wide range of parameters (e.g., in a six-layer film in the whole right region of the phase diagram of Fig. 3 calculated without the sixth-order term). At certain values of the parameters, in particular, in thicker films and in the case of the SmC^*_α phase with a wider temperature range, 180° reorientation in the center of the film occurs via an intermediate twisted structure. However, even in this case, the rotation of the tilt plane occurs mainly in the central layers of the film. It

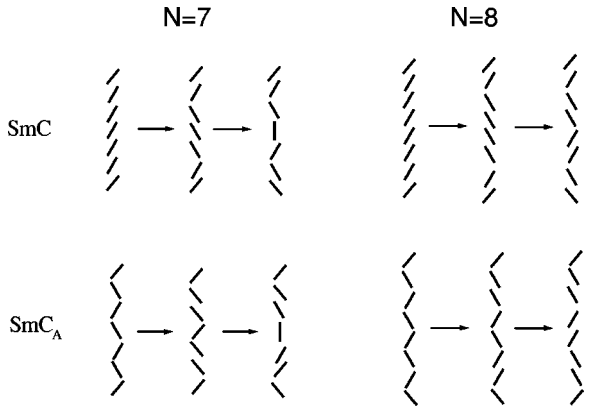

FIG. 8. Planar structures emerging from the ferroelectric and antiferroelectric phases at the surface transitions (1). At higher temperatures the transitions take place in the center of the film (2). N is the number of layers in the film. The set of model parameters is as in Fig. 2.

is worth mentioning that the symmetry consideration described above is appropriate only for the planar structures. In the twisted structures, we could only define the averaged directions of the tilt planes with respect to polarization. The behavior of the twisted structures in the electric field was investigated recently [40].

Our calculations predict not only the reorientation transitions in the center of the film, but also the possibility for the reorientation of the layers near the surfaces. These transitions can occur, in particular, in the case of the phase diagram presented in the Fig. 2 for the phase transition sequence SmC(SmC_A)-SmC_α-SmA. Figure 8 shows the transition sequence in a seven-layer and in an eight-layer film. In this case, the first reorientation takes place between the second and the third layer from the surface. The physical arguments leading to this phenomenon may be understood as follows. In comparison to the bulk, for the surface layers both the structure-stabilizing NN interactions and frustrating NNN interactions are decreased in twice, i.e., equally. For the layer nearest to the surface only the NNN interaction is decreased twice times. Thus, for the interface between the first and the second layer frustrations are weaker than for the bulk layers. The opposite is the situation for the layers next neighboring to the surface and for the interface between the second and the third layers. Due to a relatively large tilt angle θ_1 in the surface layer, the frustrated interaction [namely $(1/8)a_2\theta_1\theta_3$] can exceed the interaction stabilizing the homogeneous structure $[(1/2)a_1\theta_2\theta_3]$. This is the reason for the surface transition. At further temperature increase, likewise for the cases described above (Figs. 5 and 6) the transition in the center of the film occurs (Fig. 8). Note that the transition near the surface occurs when θ at the surface exceeds sufficiently the values of θ in the other layers. When the interlayer interactions are increased the difference between the tilt angles θ on the surface and in the interior layers is decreased. This suppresses the reorientation near the surface and the first transition takes place in the middle of the film. In the situations described in this paragraph, the first surface or the center transition occurs below the temperature range of the SmC^*_α phase in the bulk sample. We should note that the transitions near the surface do not change the symmetry of the film and consequently the polarization direction also remains unchanged.

To summarize the results of our modeling of the transitions in the thin films, we emphasize that the structures in the films can be substantially different from the structures in the bulk samples. The surface ordering, which implies a greater value of the order parameter θ on the surfaces leads not only to the shift of the phase transition temperatures, but also to an essential modification of the profile of the order parameter phase φ in the film, in particular, to the planar structure formation.

C. The effects of chirality on the pitch and subphase structures

Molecular chirality leads to a number of structural changes in SmC variant phases. We have mentioned already that at the transitions in the films (Fig. 6) chiral symmetry breaking allows a nonzero tilt in the center of N-odd films. We found that the strongest effects arise at a combined action of chirality and frustrations. In the commensurate phases, it leads to formation of the nonplanar three- and four-layer structures with a large distortion angle δ (Fig. 4). Even in the case of relatively small chirality when in the SmC^*(SmC^*_A) phase the layer-by-layer precession of the tilt angle is of the order of few degrees, the distortion angle δ may amount tens of degrees.

Usually the helicity of the SmC^*(SmC^*_A) phase is attributed to the chiral interaction, but in reality, the phase shift (i.e., rotation of the tilt plane) between the adjacent layers $\Delta\varphi=\varphi_{i+1}-\varphi_i$ not only in the SmC^*_α but also in the SmC^* phase is determined by the both chiral and frustrating interactions. In the bulk SmC^* samples near the transition to the SmA phase the ''pure chiral'' phase shift $\Delta\varphi_0$ in the absence of frustrations (i.e., at $a_2=0$) is

$$\Delta\varphi_0=\frac{2f}{\sqrt{a_1^2+4f^2}}. \tag{3.3}$$

If the both effects are included, $\Delta\varphi$ can be found from the free energy expansion as

$$\sin(\Delta\varphi-\Delta\varphi_0)=\frac{a_2}{2\sqrt{a_1^2+4f^2}}\sin 2\Delta\varphi, \tag{3.4}$$

where $\Delta\varphi_0$ is given by Eq. (3.3). Equations (3.3) and (3.4) are written in the quadratic over $\boldsymbol{\xi}$ approximation for the interlayer interactions. Near the SmC^*(SmC^*_A)-SmA phase transition and with the pitch p longer than 10^2 smectic layers, Eq. (3.4) can be brought into a more compact form

$$p=p_0(1-|a_2/a_1|), \tag{3.5}$$

where p_0 is the pitch in the absence of frustrations and $|a_2/a_1|<1$. Thus, in the presence of the chiral and frustrating interactions, a very peculiar interference phenomenon

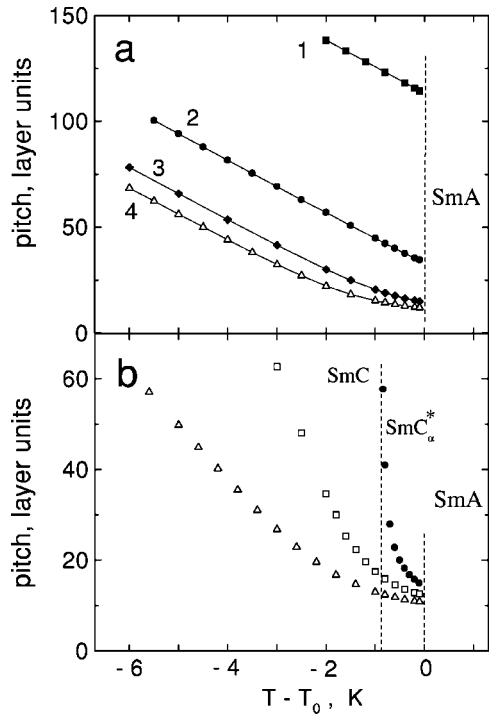

FIG. 9. Influence of the frustrating interaction a_2 and chirality f on the structure near the SmC^*($\mathrm{Sm}C^*_A$)-SmA (a) and $\mathrm{Sm}C^*_\alpha$-SmA (b) phase transitions. In (a) $a_2=0$ (curve 1), $a_2=1.5\times10^{-2}$ (curve 2), $a_2=1.75\times10^{-2}$ (curve 3), $a_2=1.85\times10^{-2}$ (curve 4). The other model parameters are $\alpha=0.01\ \mathrm{K}^{-1}$, $a_1=-1.8\times10^{-2}$, $a_3=0.05$, $f=5\times10^{-4}$. In (b) $f=0$ (closed circles), $f=2\times10^{-4}$ (open squares), $f=5\times10^{-4}$ (open triangles). The other nonzero model parameters are $\alpha=0.01\ \mathrm{K}^{-1}$, $a_1=-0.018$, $a_2=0.02$, $a_3=0.05$. Due to chirality there is no qualitative difference between the $\mathrm{Sm}C^*_\alpha$ and SmC^* phases.

between the both effects can considerably modify the helix structure. Figure 9(a) demonstrates the pitch temperature dependence (curves from 1 to 4) when the magnitude of the NNN frustrating interactions is increased. Closed symbols correspond to the case when the $\mathrm{Sm}C^*_\alpha$ phase is absent (SmC^*-SmA transition), i.e., without the chiral term the structure would be planar (the pitch is ∞). If only the chiral term is present ($a_2=0$, i.e., no frustrations) the pitch is rather large even near the transition to the SmA phase (about 115 layers, curve 1). However, at the combined action of the chirality and frustration the short-pitch structure appears near the SmC^*-SmA transition (curve 3). This phase resembles structurally the $\mathrm{Sm}C^*_\alpha$ phase, and, moreover, the temperature dependence of the pitch near the SmA phase resembles its dependence in the $\mathrm{Sm}C^*_\alpha$ phase (curve 4 was calculated at $a_1/a_2=-0.97$, i.e., when the short-pitch structure appears even without chirality).

The structural changes of the SmC^* and $\mathrm{Sm}C^*_\alpha$ phases upon increasing the chiral coefficient f are illustrated in the Fig. 9(b). At $f=0$ (i.e., without the chiral Lifshits contribution) the SmC-SmC_α phase transition manifests itself in the formation of the twisted structure [Fig. 9(b), closed symbols]. The chiral term [Fig. 9(b), curves with open symbols] leads to a nonzero twist in the whole temperature range of the tilted structures. It is worthwhile to remind the cholesteric-nematic phase transition where even an infinitesimal small chiral contribution induces helical orientational ordering (although with a huge pitch). In this case, strictly speaking, one cannot say where the transition occurs, as the symmetry of the phases is the same, and a smooth temperature change of the order parameter modulus and phase takes place. Such a continuous evolution of the pitch and of the layer spacing (and hence the tilt angle) was observed recently in the temperature region of the SmC^* and $\mathrm{Sm}C^*_\alpha$ phases [21]. Experimental observations and our calculations state the question what in reality is the $\mathrm{Sm}C^*_\alpha$ phase in a chiral compound: a distinct phase, a short-pitch variation of the SmC^*($\mathrm{Sm}C^*_A$) phase or in different compound, we are dealing with qualitatively different structures. This question goes beyond the scope of our model, however, such a problem should obviously hold for other chiral frustrated systems.

IV. CONCLUSIONS

Investigations of polar smectic liquid crystals are not only interesting for basic research but also for modern electronic and material science applications. However, for a long time not only the structures of subphases were not known, but even suitable methods of their determination were not developed, and theoretical interpretations were rather obscured. Recent x-ray and optical investigations demonstrated that spatial modulation of the order parameter phase φ governs the structure of these phases.

The message of our paper is that the main features of these complex structures may be derived from the relatively simple free energy expansion including just the interactions of the nearest and of the next-nearest layers. Lacking sufficient data on the interaction parameters one can at present reasonably discuss only the general features of the polar smectic structures and therefore, we include in our model only the terms necessary to capture the correct shape and topology of the phase diagrams. Our calculations are rather economic in time, and the agreement with experiments indicates that we are on the right track.

We examined the layer-by-layer dependence of the order parameter phase in three-layer and four-layer structures (information about which was obtained from optical data), and the spatial modulation of the order parameter modulus in the three-layer subphase (in this respect, the present paper supplements our recent study [31]). Our calculations predict as well the formation of the six-layer structure. Since this phase is emerging from the same form of the free energy as the already observed three- and four- layers structures, no reasons can be seen why the six-layer structure would not also exist.

Even for the simple smectic structures, where in the bulk sample the phase of the order parameter does not play any essential role, confined geometry leads to formation of nontrivial structures [41]. Due to the coupling between the modulus and the phase of the order parameter, the short-pitch structure observed at constant θ in the bulk, may become

unstable in the case of nonconstant θ in smectic films. Owing to the surface ordering, θ is minimal in the center of the film. Because the NNN frustrating interaction has a longer range with respect to the interaction stabilizing synclinic or anticlinic structures, it includes the layers with greater value of θ. According to this, the frustration energy in the center of the film may exceed the energy stabilizing the homogeneous orientation. This leads to the reorientation in the center of the film. Another ''weak point'' in the film where the reorientation may take place, is the interface between the second and the third layer from the surface. At these transitions the surface layers preserve their orientations. Even more complex are nonplanar structures with nonhomogeneous profile of the order parameter. It was established long ago that the order parameter of Sm*C* liquid crystals is a two-component vector. However, a real manifestation of this feature was found relatively recently in the structures of smectic polar subphases.

The experimental situation is now changing, and techniques in the film preparation and in optical and x-ray measurements progress to the point where tiny details of the structures can be measured with a high accuracy. Further experimental and theoretical investigations are required for revealing the detailed structure of subphases and relations of microscopic interactions to their macroscopic properties.

ACKNOWLEDGMENTS

This work was supported by the Russian Foundation for Basic Research Grant No. 01-02-16507. One of us (E.K.) is indebted to INTAS (Grant No. 01-0105) for partial support.

[1] A.D.L. Chandani, E. Gorecka, Y. Ouchi, H. Takezoe, and A. Fukuda, Jpn. J. Appl. Phys., Part 2 **28**, L1265 (1989).
[2] A. Fukuda, Y. Takanishi, T. Isozaki, K. Ishikawa, and H. Takezoe, J. Mater. Chem. **4**, 997 (1994).
[3] R.B. Meyer, L. Liébert, L. Strzelecki, and P. Keller, J. Phys. (France) Lett. **36**, L69 (1975).
[4] P. Mach, R. Pindak, A.-M. Levelut, P. Barois, H.T. Nguyen, C.C. Huang, and L. Furenlid, Phys. Rev. Lett. **81**, 1015 (1998).
[5] P. Mach, R. Pindak, A.-M. Levelut, P. Barois, H.T. Nguyen, H. Baltes, M. Hird, K. Toyne, A. Seed, J.W. Goodby, C.C. Huang, and L. Furenlid, Phys. Rev. E **60**, 6793 (1999).
[6] P.M. Johnson, S. Pankratz, P. Mach, H.T. Nguyen, and C.C. Huang, Phys. Rev. Lett. **83**, 4073 (1999).
[7] D. Schlauf, Ch. Bahr, and H.T. Nguyen, Phys. Rev. E **60**, 6816 (1999).
[8] D.A. Olson, S. Pankratz, P.M. Johnson, A. Cady, H.T. Nguyen, and C.C. Huang, Phys. Rev. E **63**, 061711 (2001).
[9] Y. Takanishi, K. Hiraoka, V. Agrawal, H. Takezoe, A. Fukuda, and M. Matsushita, Jpn. J. Appl. Phys., Part 1, **30**, 2023 (1991).
[10] T. Isozaki, T. Fujikawa, H. Takezoe, A. Fukuda, T. Hagiwara, Y. Suzuki, and I. Kawamura, Phys. Rev. B **48**, 13 439 (1993).
[11] T. Akizuki, K. Miyachi, Y. Takanishi, K. Ishikawa, H. Takezoe, and A. Fukuda, Jpn. J. Appl. Phys., Part 1 **38**, 4832 (1999).
[12] S.A. Pikin, S. Hiller, and W. Haase, Mol. Cryst. Liq. Cryst. Sci. Technol., Sect. A **262**, 425 (1995).
[13] S.A. Pikin, M. Gorkunov, D. Kilian, and W. Haase, Liq. Cryst. **26**, 1107 (1999).
[14] M. Gorkunov, S. Pikin, and W. Haase, JETP Lett. **72**, 81 (2000).
[15] M. Čepič and B. Žekš, Mol. Cryst. Liq. Cryst. Sci. Technol., Sect. A **263**, 61 (1995).
[16] A. Roy and N.V. Madhusudana, Europhys. Lett. **36**, 221 (1996).
[17] B. Rovšek, M. Čepič, and B. Žekš, Phys. Rev. E **54**, R3113 (1996).
[18] A. Roy and N.V. Mathusudana, Europhys. Lett. **41**, 501 (1998).
[19] B. Rovšek, M. Čepič, and B. Žekš, Phys. Rev. E **62**, 3758 (2000).
[20] A. Cady, D.A. Olson, X.F. Han, H.T. Nguyen, and C.C. Huang, Phys. Rev. E **65**, 030701 (2002).
[21] L.S. Hirst, S.J. Watson, H.F. Gleeson, P. Cluzeau, P. Barois, R. Pindak, J. Pitney, A. Cady, P.M. Johnson, C.C. Huang, A.-M. Levelut, G. Srajer, J. Pollmann, W. Caliebe, A. Seed, M.R. Herbert, J.W. Goodby, and M. Hird, Phys. Rev. E **65**, 041705 (2002).
[22] A. Fera, R. Opitz, W.H. de Jeu, B.I. Ostrovskii, D. Schlauf, and Ch. Bahr, Phys. Rev. E **64**, 021702 (2001).
[23] P.V. Dolganov, Y. Suzuki, and A. Fukuda, Phys. Rev. E **65**, 031702 (2002).
[24] P.V. Dolganov, E.I. Demikhov, Y. Suzuki, and A. Fukuda, Zh. Eksp. Teor. Fiz. **122**, 840 (2002) [JETP **95**, 728 (2002)].
[25] V.K. Dolganov, E.I. Kats, and S.V. Malinin, Zh. Eksp. Teor. Fiz. **120**, 609 (2001) [JETP **93**, 533 (2001)].
[26] I. Muševič, R. Blinc, and B. Žekš, *The Physics of Ferroelectric and Antiferroelectric Liquid Crystals* (World Scientific, Singapore, 2000).
[27] M. Čepič and B. Žekš, Phys. Rev. Lett. **87**, 085501 (2001).
[28] M.A. Osipov and A. Fukuda, Phys. Rev. E **62**, 3724 (2000).
[29] T. Stoebe, L. Reed, M. Veum, and C.C. Huang, Phys. Rev. E **54**, 1584 (1996).
[30] R.H. Byrd, P. Lu, and J. Nocedal, SIAM (Soc. Ind. Appl. Math.) J. Sci. Stat. Comput. **16**, 1190 (1995).
[31] P.V. Dolganov, V.M. Zhilin, V.E. Dmitrienko, and E.I. Kats, Pis'ma Zh. Eksp. Teor. Fiz. **76**, 579 (2002) [JETP Lett. **76**, 498 (2002)].
[32] D.A. Olson, X.F. Han, A. Cady, and C.C. Huang, Phys. Rev. E **66**, 021702 (2002).
[33] E. Gorecka, D. Pociecha, M. Čepič, B. Žekš, and R. Dabrowski, Phys. Rev. E **65**, 061703 (2002).
[34] D. Konovalov, H.T. Nguyen, M. Čopič, and S. Sprunt, Phys. Rev. E **64**, 010704(R) (2001).
[35] S. Heinekamp, R.A. Pelcovits, E. Fontes, E.Y. Chen, R. Pindak, and R.B. Meyer, Phys. Rev. Lett. **52**, 1017 (1984).
[36] B. Rovšek, M. Čepič, and B. Žekš, Mol. Cryst. Liq. Cryst. Sci. Technol., Sect. A **329**, 365 (1999).
[37] K. Miyachi, J. Matsushima, Y. Takanishi, K. Ishikawa, H. Tak-

ezoe, and A. Fukuda, Phys. Rev. E **52**, R2153 (1995).
[38] D.R. Link, J.E. Maclennan, and N.A. Clark, Phys. Rev. Lett. **77**, 2237 (1996).
[39] D.R. Link, G. Natale, N.A. Clark, J.E. Maclennan, M. Walsh, S.S. Keast, and M.E. Neubert, Phys. Rev. Lett. **82**, 2508 (1999).
[40] M. Conradi, I. Muševič, and M. Čepič, Phys. Rev. E **65**, 061705 (2002).
[41] See, e.g., Ch. Bahr, Int. J. Mod. Phys. B **8**, 3051 (1994); T. Stoebe and C.C. Huang, *ibid.* **9**, 2285 (1995).